Nonresonant optical control of a spinor polariton condensate

A. Askitopoulos,[1,*] K. Kalinin,[2] T. C. H. Liew,[3] P. Cilibrizzi,[1] Z. Hatzopoulos,[4,5] P. G. Savvidis,[4,6] N. G. Berloff,[2,7] and P. G. Lagoudakis[1,†]

[1]*Department of Physics & Astronomy, University of Southampton, Southampton, SO17 1BJ, United Kingdom*
[2]*Skolkovo Institute of Science and Technology, Novaya St., 100, Skolkovo 143025, Russian Federation*
[3]*School of Physical and Mathematical Sciences, Nanyang Technological University, 637371, Singapore*
[4]*Microelectronics Research Group, IESL-FORTH, P.O. Box 1527, 71110 Heraklion, Crete, Greece*
[5]*Department of Physics, University of Crete, 71003 Heraklion, Crete, Greece*
[6]*Department of Materials Science and Technology, University of Crete, Crete, Greece*
[7]*Department of Applied Mathematics and Theoretical Physics, University of Cambridge, Wilberforce Road, Cambridge CB3 0WA, United Kingdom*

(Received 10 November 2015; revised manuscript received 16 February 2016; published 20 May 2016)

We investigate the spin dynamics of polariton condensates spatially separated from and effectively confined by the pumping exciton reservoir. We obtain a strong correlation between the ellipticity of the nonresonant optical pump and the degree of circular polarization (DCP) of the condensate at the onset of condensation. With increasing excitation density we observe a reversal of the DCP. The spin dynamics of the trapped condensate are described within the framework of the spinor complex Ginzburg-Landau equations in the Josephson regime, where the dynamics of the system are reduced to a current-driven Josephson junction. We show that the observed spin reversal is due to the interplay between an internal Josephson coupling effect and the detuning of the two projections of the spinor condensate via transition from a synchronized to a desynchronized regime. These results suggest that spinor polariton condensates can be controlled by tuning the nonresonant excitation density offering applications in electrically pumped polariton spin switches.

DOI: 10.1103/PhysRevB.93.205307

I. INTRODUCTION

Implementation of all optical, integrable spin-polarization switching devices is one of the essential ingredients for the realization of novel solid-state optoelectronic spin-logic architectures [1]. Semiconductor microcavities, operating in the strong coupling regime, have recently emerged as ideal systems for achieving this goal due to their inherent spin multistabilities [2,3] and fast spin dynamics [4,5] that arise from their strong optical nonlinearities [6]. Exciton-polaritons, the eigenstates of these systems, are bosonic light-matter quasiparticles that inherit the spin properties of their exciton component, while their decay gives rise to photons with a polarization defined by the polariton spin. This robust spin to photon polarization conversion is favorable for fast nondestructive readout of the spin state of the system. Moreover, the advancement of fabrication techniques has yielded microcavity structures of high finesse featuring polariton lifetimes of the order of tens of picoseconds [7], enabling the emergence of optically excited polariton lasing and condensation [8,9] even at room temperature [10]. In state of the art microcavity structures, polariton condensates propagate ballistically [11] and this has enabled the first demonstrations of polariton condensate optical switches [12–14].

Initial realizations of resonant polariton spin switches [15], followed by experimental demonstrations of extensive polariton spin transport in planar [16] as well as 1D structures [17], has emphasized the potential of theoretical propositions for fully integrated polariton based spin circuits[18,19]. The short lifetime of polaritons considered to be an impediment for thermodynamic equilibrium and bosonic condensation can now be seen as an advantage in creating ultra-fast spin switching devices. In this regard, as nonresonant excitation schemes more closely resemble polariton formation under electrical injection, they hold greater promise for the implementation of electrically controlled polariton spin logic devices. This remarkable possibility has been further highlighted by the recent development of novel electrically pumped polariton lasers [20,21].

In polarization resolved experiments under resonant excitation [15], parametric amplification [4] as well as in the OPO configuration [5,22], correlations between the polarization of the excitation beam and the resulting polariton spin have been extensively studied. In Refs. [3,23], the emergence of a circularly polarized condensate was observed at near-resonant linearly polarized optical excitation. For nonresonant excitation, prior studies have demonstrated that upon condensation, the polarization of the condensate is pinned to the crystallographic axis of the microcavity structure independent of the exciting polarization [24]. This effect has been originally attributed to a linear polarization splitting of $\approx$0.1 meV (at $k_{\parallel} = 0$), disputing that the emission polarization is inherited from the excitation [24]. The spontaneous emergence of a strong linear polarization upon condensation threshold has in-fact been treated as a suitable order parameter for determining the emergence of coherence in the system [25,26]. However, in more recent experiments, a higher total degree of polarization was reported under circularly polarized nonresonant pulsed excitation rather than for linearly polarized excitation [27]. Moreover, in polariton spin textures generated under circularly polarized excitation, a high DCP was reported in the vicinity of the pump spot [16,17]. These experiments confirmed that

*alexis.askitopoulos@soton.ac.uk
†pavlos.lagoudakis@soton.ac.uk

there are correlations between the polarization of the optical excitation with the polarization of the condensate, which in GaAs/AlGaAs MCs are not screened from optical disorder.

In this paper, we demonstrate that the spin imbalance in a polariton condensate can be vigorously modulated by the polarization properties of the nonresonant excitation beam when the polariton condensate and exciton reservoir are spatially separated. In the nonlinear regime, we observe a strong linear to circular polarization conversion controlling the condensate polarization by tuning the angle of the linear polarization of the excitation beam. Moreover, the condensate density is shown to strongly effect the resulting spin imbalance leading to a spin reversal at high densities. We explain this reversal within the framework of a coherent internal Josephson coupling mechanism between the overlapping spin states of the condensate and present results of analytical approximations and numerical simulations that closely reproduce the experiment. These experiments confirm that the polarization of nonresonant excitation indeed survives the relaxation mechanisms from electron and holes to polaritons and its effects are exacerbated when the strong interactions from the reservoir are spatially decoupled. Furthermore, internal Josephson coupling effects between spin-up and spin-down coherent states are demonstrated to be an important factor governing the polarization build up in the condensate.

II. EXPERIMENTAL RESULTS

To study the polarization properties of a polariton condensate, we utilize the optical trap configuration from our previous work [28]. Using a nonresonant continuous wave (CW) linearly polarized pump spatially shaped in the form of an annular ring and focused on the sample surface through a 0.4 numerical aperture (NA) objective, we create the Ψ_{00} coherent state in the optically induced trap, as shown schematically in Fig. 1(a) [29]. The S_+ and S_- components of the emission below and above threshold are resolved with the use of a $\lambda/4$ wave plate and a linear polarizer and are then used to reconstruct a real-space image of the S_z stokes component [30]. We used a high-Q (16 000) $5\lambda/2$ microcavity with a cavity lifetime of $\sim$7 ps composed of GaAs/AlGaAs DBRs, while the cavity is embedded with four triplets of 10-nm GaAs quantum wells with $Al_{0.3}Ga_{0.7}As$ barriers.

Below threshold we do not detect any significant circular polarization from polaritons inside the trap, shown on Fig. 1(b), however, just above the threshold, we detect a strong circularly polarized emission of about 0.6 DCP as shown in Fig. 1(c). This is in stark contrast with the linear polarization build-up previously reported for polariton condensates [24]. It is worth noting that the circular component originates from the emission of the condensate while the DCP of the surrounding excitation region, where polaritons interact with the incoherent reservoir is negligible. Interestingly, this strong S_z stoke component persists far from the peak of the condensate and exhibits a DCP > 0.5 even where the condensate intensity is 10% of its peak intensity as shown in Fig. 1(d).

Although the emergence of a strong spin imbalance from a linearly polarized optical pump appears counterintuitive, it can, nevertheless, be interpreted if one takes into account that the polarization of a monochromatic tightly focused optical

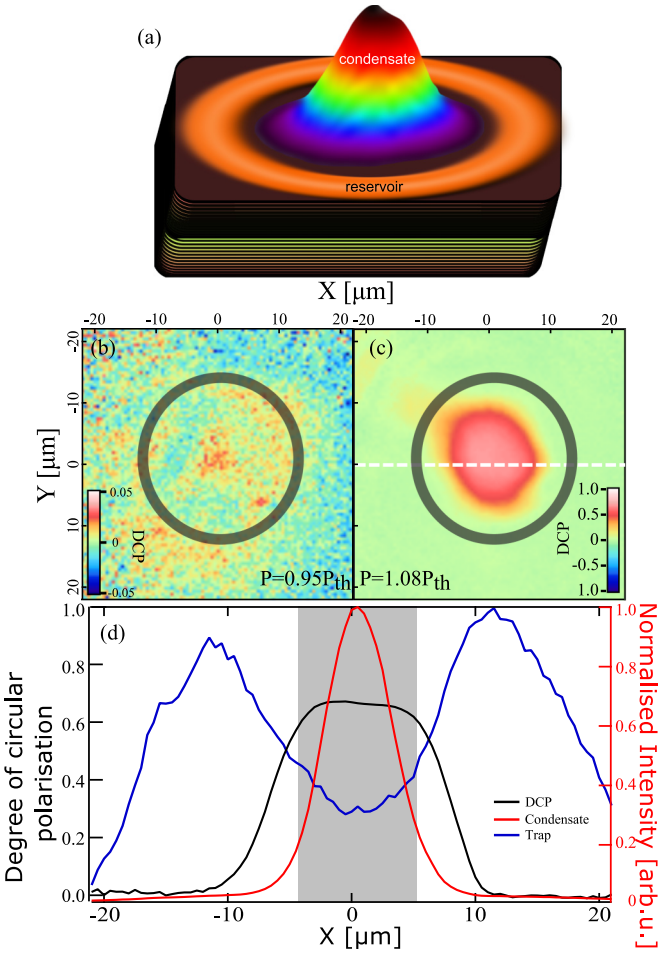

FIG. 1. (a) Schematic representation of reservoir and condensate in the microcavity. Real space map of the degree of circular polarization (b) below ($P = 0.95P_{\text{th}}$), and (c) above ($P = 1.08P_{\text{th}}$) condensation threshold. (d) Normalized intensity of the polariton emission above threshold (red line, right axis), below threshold (blue line, right axis) and DCP (black line, left axis) across the white dotted line profile of (c).

field does not have a uniform polarization. For high numerical aperture lenses, scalar diffraction geometry is insufficient to accurately describe the electromagnetic field in the focal plane and a vectorial analysis of light is required in order to precisely describe the electromagnetic field in the focal plane [31]. Indeed, it is a well studied effect that the electric field in the focal plane of a high numerical aperture aplanatic system can induce a small degree of ellipticity even for a 100% linearly polarized source [32,33]. In our setup, the microscope objective (NA = 0.4), yields a measured DCP at the center of a focused linearly polarized beam of 0.1 [34]. Moreover, this ellipticity is calculated to be greater towards the periphery of the focal plane, where our ringlike excitation pattern is found, than in the central region [31].

The ellipticity of the pump does not play an important role below threshold where the emission is stronger in the excitation region. Indeed, it has been predicted that spin noise fluctuations are extremely sensitive to the statistics and occupation number in polariton systems [35]. Therefore, in the incoherent state, a small spin imbalance (pump with small ellipticity) in the

injection of carriers is not expected to have a noticeable effect in the polarization of the emission. This has been demonstrated even for fully circular optical excitation schemes [27]. However, upon crossing the condensation threshold, a drastically different picture emerges. Spin fluctuations are greatly suppressed [35] and density dependent bosonic amplification favours the polariton spin state with higher occupation. In the absence of any spin relaxation mechanism between $S_\uparrow$ and $S_\downarrow$ polaritons, the bosonic amplification of the dominant spin population gives rise to a strongly circularly polarized polariton condensate. Furthermore, the spatial separation of the condensate from the exciton reservoir amplifies this behavior as the spin decoherence channels associated with polaritons interacting with particles within the reservoir are considerably suppressed [28]. In excitation schemes where the reservoir is spatially overlapped with the condensate (e.g. top hat or Gaussian spot excitation) the scattering processes within the reservoir suppress externally imposed spin imbalances. However, even in such cases, careful analysis of the spatiotemporal polarization dynamics have shown spin phenomena that are driven by the spin imbalance in the exciton reservoir, such as polariton spin whirls and intricate spin textures [34,36].

In order to further characterize the origin of the circular polarization in the condensate it is meaningful to establish whether it is isotropic and independent of the angle of the linear polarization of the optical pump. To achieve this, we initialize the condensate above threshold ($P = 1.1P_{\text{th}}$) as before and using a half-wave plate we rotate the linear polarization of the excitation. Figure 2(a) displays the spatial profile of the DCP

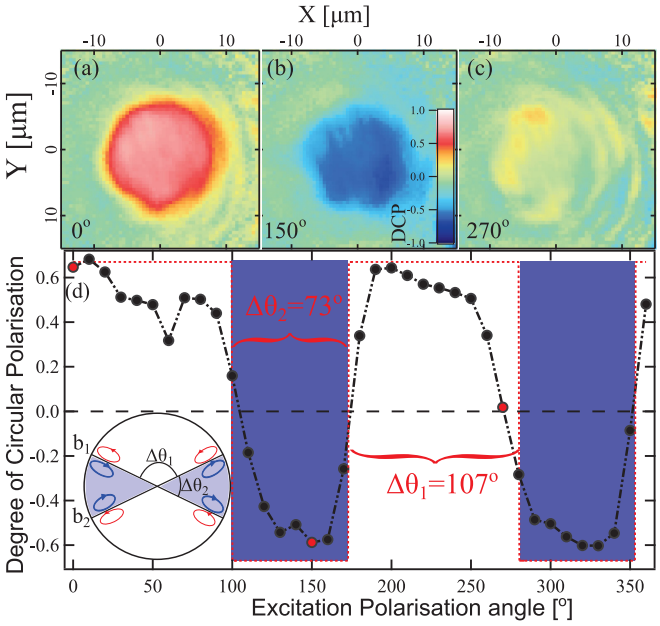

FIG. 2. Variation of the condensate's DCP with the linear polarization angle of the excitation beam. Circular polarization maps of the confined polariton condensate just above threshold for linear polarization angle: (a) $\theta = 0°$, (b) 150°, and (c) 270°. (d) The average DCP is plotted vs external polarization angle featuring a 2θ dependence (red dots mark the data at the above angles). (Inset) Schematic representation of the induced ellipticity to the excitation beam vs the linear polarization angle.

under horizontal (0°) linear excitation showing a high DCP in the emission. Rotating the angle initially has a marginal effect on the circular stokes component of the condensate. However, for polarization rotation above 90°, the DCP is reduced eventually leading to a complete reversal of the polarization at 130° as shown in Fig. 2(b). After 180° rotation of the linear polarization angle the condensate has regained its original polarization. Figure 2(c) shows the spatial DCP near the tipping point. In this regime it has been shown that individual realizations of the trapped condensate are stochastically spin up or spin down [37]. Furthermore, perturbation of the system by a polarized femtosecond pulse can also induce temporary as well as permanent spin flips [37,38], depending on the polarization of the pulse and of the trapped condensate. The DCP of the system has almost a 2θ relation with the angle of the linear polarization of the excitation, shown in Fig. 2(d), where the value of each point is the average of the DCP in the central region of the condensate.

The demonstrated 2θ dependence on the angle of the excitation polarization is an indication of optical anisotropy present in the sample. Light focused on the surface of the sample propagates through the top DBR mirror, where there is no absorption for the excitation wavelength ($\lambda_{\text{laser}} = 752$ nm), before exciting the excitons in the QWs. In our sample, the DBR consists of pairs of AlAs/$Al_{0.3}Ga_{0.7}As$ layers for which there have been a number of works, for similar multilayered structures reporting linear birefringence [39–41]. The birefringence in the DBR will therefore exacerbate the ellipticity of the excitation beam and result in the 2θ dependence. Therefore the observed symmetry breaking at threshold is explicit, brought about by the imbalance in the population of $S_{\uparrow,\downarrow}$ particles. However, when the ellipticity induced by the objective is counterbalanced by the birefringence of the sample, any appearance of circular polarization becomes implicit to the system (spontaneous symmetry breaking) [37].

In the previously discussed results, the excitation power of the nonresonant, nonlocal pump and therefore the condensate density was kept constant ($P = 1.1 \times P_{\text{th}}$). In polariton condensates, increasing the density has been shown to have a strong impact on its polarization through the increase of spin-dependent polariton-polariton interactions that tend to depolarize the emission [27,42]. We investigate the condensate density dependence in a polarization resolved power dependent experiment. Further increase of the density above threshold initially results in reducing the DCP of the emission. However, at 2.2 times the threshold power we observe a reversal of the DCP and thus of the polariton pseudospin Fig. 3(a). It is worth noting here that we do not observe any deviation from the ground state of the trap within the power range that we studied. This is demonstrated in the inset of Fig. 3(a) that shows the real-space 1D profile of the two spin components of the condensate with respect to power over threshold. Figure 3(b) depicts the power dependence of a spatial cross-section of the emission for increasing power, while the black line denotes the photoluminescence from the trap barriers below threshold that outlines the trap profile. The points of Fig. 3(a) are taken from the point of maximum intensity of the condensate ($I_\uparrow + I_\downarrow$). Due to the intensity nonlinearity, inherent in polariton condensation, the signal to noise ratio (SNR) that we record from the condensate

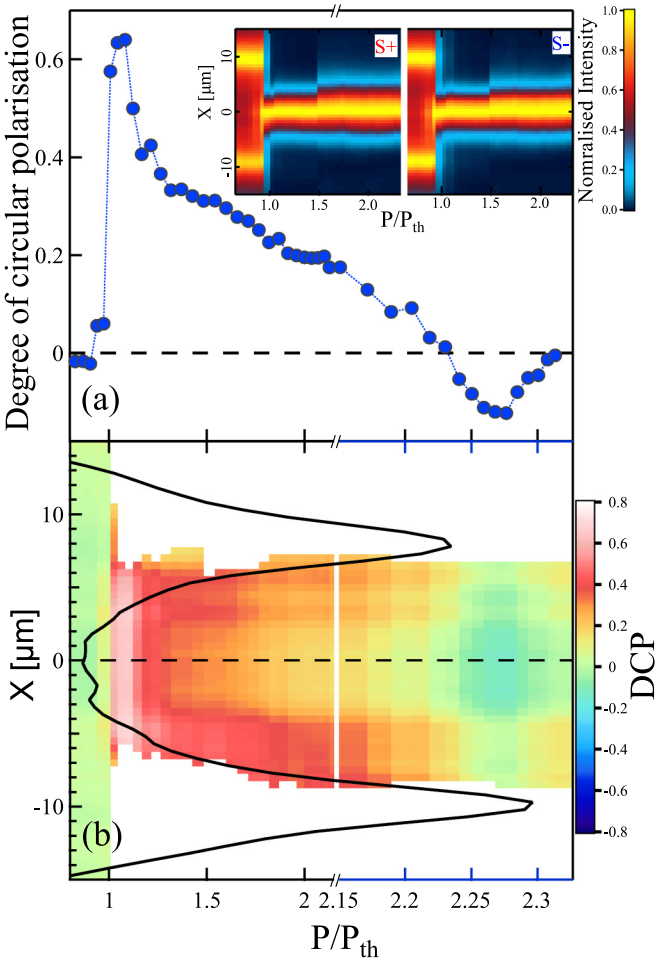

FIG. 3. (a) DCP as a function of excitation power vs threshold power. (b) Power dependence vs a spatial cross-section of the DCP across the trap. Note the change in scale at 2.15. The figure shows the region where SNR $\geqslant$ 1 dB. The black line outlines the emission below threshold defining the trap. The inset in (a) shows the two normalized spin components of the 1D real-space profile of the condensate with respect to power above threshold.

(8.75 dB $\leqslant$ SNR$_c$ $\leqslant$ 14 dB) is much greater than that at the excitation region (SNR$_{\text{res}} \approx 0.1$ dB). In Fig. 3(b), we plot the DCP in the region of confidence where SNR $\geqslant$ 1 dB. The spin reversal dependence of a polariton condensate with excitation density under nonresonant optical pumping cannot be described within the framework of the linear optical spin Hall effect [43].

III. JOSEPHSON COUPLING MODEL

Our theoretical model consists of a system of spinor Ginzburg-Landau equations (GLE) [44] written in the basis of left- and right-circular polarized polariton wave functions (spin-up and spin-down), denoted by $\psi_\pm$:

$$i\hbar\frac{\partial\psi_\pm}{\partial t} = \left[-\frac{\hbar^2}{2m}\nabla^2 + U_0|\psi_\pm|^2 + (U_0 - 2U_1)|\psi_\mp|^2 + \hbar g_R n_\pm + \frac{i\hbar}{2}(R_R n_\pm - \gamma_C)\right]\psi_\pm + \Omega\psi_\mp, \quad (1)$$

where in the Hamiltonian part of the equations we take into account an interaction with the total polariton density $H_{U_0} = U_0/2(|\psi_+|^2 + |\psi_-|^2)^2$ as well as an attractive interaction between opposite spin species, $H_{U_1} = -2U_1|\psi_+|^2|\psi_-|^2$, and the symmetry-breaking term $H_\Omega = \Omega(\psi_+\psi_-^* + \text{H.c.})$, which arises due to asymmetry at the quantum-well interfaces, mechanical stresses, or due to the anisotropy-induced splitting of linear polarisations in the microcavity. Josephson coupling has been extensively studied and experimentally observed in polariton condensates, both in the intrinsic case [23,45] as well as the extrinsic case [46–50]. In this model, there is no explicit dependence on the shape of the pump, nevertheless the symmetry breaking term H_Ω, appears exactly because the interactions with the reservoir are filtered out due to the geometry of the experiment [51]. The rate equation for the reservoir represents the evolution of the exciton densities $n_\pm$ is

$$\frac{\partial n_\pm(\mathbf{r},t)}{\partial t} = -(\gamma_R + R_R|\psi_\pm|^2)n_\pm(\mathbf{r},t) + P_\pm(\mathbf{r},t), \quad (2)$$

where we have neglected the hot excitons diffusion and advection. In Eqs. (1) and (2), γ_R and γ_C are the reservoir and condensate decay rates, respectively, R_R is the scattering rate to/from reservoir, $P_\pm$ is the pumping rate and g_R is the condensate blueshift from interactions with reservoirs.

A. Two-mode model

We nondimensionalize (1) and (2), neglect the spatial variation of all parameters and obtain the following ccGLEs and rate equations:

$$2i\frac{\partial\psi_\pm}{\partial t} = \left[|\psi_\pm|^2 + (1 - U_\alpha)|\psi_\mp|^2 + gn_\pm + \frac{i}{2}(Rn_\pm - 1)\right]\psi_\pm + J\psi_\mp, \quad (3)$$

$$2\frac{\partial n_\pm}{\partial t} = -(\gamma + b|\psi_\pm|^2)n_\pm + p_\pm, \quad (4)$$

where the following dimensionless parameters were used [51]:

$$U_\alpha = 2\frac{U_1}{U_0};\quad g = \frac{2mg_R}{\hbar};\quad R = \frac{2mR_R}{\hbar};\quad J = \frac{\Omega}{\hbar\gamma_C};$$
$$\gamma = \frac{\gamma_R}{\gamma_C};\quad b = \frac{\hbar R_R}{U_0};\quad p_\pm = \frac{\hbar}{2m\gamma_C^2}P_\pm. \quad (5)$$

These equations can be conveniently reparametrized using

$$\psi_\pm = \sqrt{\rho_\pm}e^{i(\phi\pm\frac{\Theta}{2})},\quad \rho = \frac{\rho_+ + \rho_-}{2},\quad z = \frac{\rho_+ - \rho_-}{2}, \quad (6)$$

where $\rho_\pm$ are the densities of polaritons with spin-up and spin-down, ϕ is the global phase which does not have an influence on our solution due to nonresonant incoherent pump, Θ is the phase difference between the polaritons of different species, ρ is the averaged density. Separating real and imaginary parts gives the coupled equations for Θ, ρ, and z:

$$\dot\Theta = -U_\alpha z - \frac{g}{2}(n_+ - n_-) + \frac{Jz\cos\Theta}{\sqrt{\rho^2 - z^2}},$$
$$\dot z = \frac{R}{4}(n_+(\rho + z) - n_-(\rho - z)) - J\sqrt{\rho^2 - z^2}\sin\Theta - \frac{z}{2},$$
$$\dot\rho = \frac{R}{4}(n_+(\rho + z) + n_-(\rho - z)) - \frac{\rho}{2}, \quad (7)$$

where, in the view of the fast reservoir relaxation in comparison with the condensate relaxation ($\gamma \approx 10$ [52–54]) we replaced Eq. (4) with the equilibrium values

$$n_{\pm} = \frac{p_{\pm}}{\gamma + b(\rho \pm z)}. \tag{8}$$

We are interested in the resulting degree of the circular polarization, $\xi = z/\rho$, assuming a small discrepancy in the pumping $\eta = p_+/p_- > 1$.

B. Josephson regime

The behavior of the system [Eqs. (7)] can be understood by considering the so-called Josephson regime: $J \ll U_\alpha \rho$, $z \ll \rho$, and where we consider a small pumping discrepancy $\eta = 1 + \epsilon$, where $\epsilon \ll 1$. Equation (7) reduces to an equation for a driven damped pendulum (or a current-based Josephson junction):

$$\ddot{\Theta} + \left(\frac{1}{2} - \frac{\gamma}{2Rp_-(1+\epsilon)}\right)\dot{\Theta} = -U_\alpha \frac{\rho_{\rm st}\epsilon}{2(2+\epsilon)} + J\rho_{\rm st}\left(U_\alpha - \frac{gb}{(1+\epsilon)R^2 p_-}\right)\sin\Theta, \tag{9}$$

where the density $\rho_{\rm st}$ corresponds to the stationary case (a Bloch surface):

$$\rho_{\rm st} = \frac{(\epsilon+2)Rp_- - 2\gamma}{2b}. \tag{10}$$

The behavior of the driven damped pendulum has been studied in detail [55]. Depending on the sign of the driving amplitude $A = J\rho_{\rm st}[U_\alpha - gb/(1+\epsilon)R^2 p_-]$ the "pendulum" acts to drive Θ to either 0 (if $A > 0$) or to π (if $A < 0$). The first term on the right-hand side of Eq. (10) represents a constant driving torque. The threshold condition for condensation is $\gamma/Rp_- < 1$, so the second term on the left-hand side of Eq. (10) represents damping with a rate $\alpha = (1 - \gamma/Rp_-(1+\epsilon))/2$ that grows from the threshold approaching 1/2. We transform Eq. (10) into a set of the first-order equations:

$$\dot{\Theta} = \chi, \quad \dot{\chi} = -\alpha\chi - U_\alpha \frac{\rho_{\rm st}\epsilon}{2(2+\epsilon)} + A\sin\Theta. \tag{11}$$

From the analysis of this system it is clear that depending on the values of the coefficients the trajectory of the system is attracted to either a fixed point or a limit cycle. A stable fixed point exists if

$$U_\alpha \frac{\epsilon}{2(2+\epsilon)} \leqslant J\left|U_\alpha - \frac{gb}{(1+\epsilon)R^2 p_-}\right|. \tag{12}$$

We can refer to the corresponding fixed point solution as a synchronized solution since the relative phase of two components becomes fixed in time. If this condition is not satisfied, there is no fixed point and the relative phase between the components evolves periodically. We will refer to this regime as a desynchronized solution.

The desynchronization occurs when Eq. (12) is violated, which for small epsilon occurs when

$$\epsilon > 4J\left|1 - \frac{gb}{U_\alpha R^2 p_-}\right|, \tag{13}$$

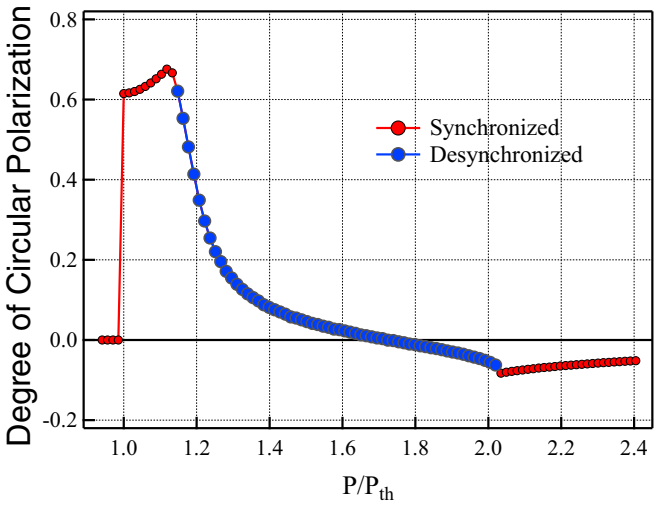

FIG. 4. The degree of circular polarization, ξ, as a function of the pumping strength $P/P_{\rm th}$ obtained by numerical integration of Eq. (7). The blue dots correspond to the desynchronized state where the polarization degree and condensate density are oscillating in time (the values of these functions are averaged over the period of their oscillation), the red dots corresponds to fixed points. Even for a small discrepancy in the pumping intensity, the degree of the circular polarization can vary from elliptical polarization to linear polarization to polarization reversal. The parameters used are $\gamma = 10$, $g = 0.7$, $b = 15$, $R = 1.0$, $U_\alpha = 1.1$, $J = 0.045$, and $\eta = 1.1$.

and in terms of the pumping takes place around

$$p_- \approx \frac{gb}{U_\alpha R^2}. \tag{14}$$

C. Spin reversal

The presence of the internal Josephson coupling term J is essential for obtaining the spin reversal. If $J = 0$, then the equation on the relative phase Θ in Eq. (7) becomes decoupled from the rest of the system. The regime for negligible J is relevant when the reservoir shields the condensate from the mechanical stresses and asymmetries of the underlying crystal (for instance for a single spot excitation). As the pumping strength grows the condensate enters the desynchronized regime, which leads to small z getting close to the linearly polarized state. If J is nonzero, as one would expect for trapped condensates, the fixed point $\dot{\Theta} = 0$ in the Josephson regime requires z to take negative values $z \approx -g(n_+ - n_-)/2U_\alpha$. Therefore the transition from the synchronized regime at low pumping to desynchronized at higher pumping makes it possible for the system to reach the linear polarized state. The transition to a steady state is not possible without polarization spin flip. To verify this analysis, we integrate Eq. (7) and show the dependence of the DCP, ξ, on the pumping strength, $p = p_-$, over the threshold in Fig. 4.

IV. FULL SYSTEM

Finally, we check the dynamics of the DCP for a trapped condensate without neglecting the spatial variation. We

solve

$$2i\frac{\partial\psi_\pm}{\partial t} = \Big[-\nabla^2 + |\psi_\pm|^2 + (1-U_\alpha)|\psi_\mp|^2 + gn_\pm + \frac{i}{2}(Rn_\pm - 1)\Big]\psi_\pm + J(\mathbf{r})\psi_\mp, \quad (15)$$

$$n_\pm(\mathbf{r}) = \frac{p_\pm(\mathbf{r})}{\gamma + b|\psi_\pm|^2}, \quad (16)$$

where the pumping profile p_- and the internal Josephson coupling J are given by

$$p_-(\mathbf{r}) = P\exp[-\alpha(r-r_0)^2],$$
$$J(\mathbf{r}) = \min(J_{\max}, 1/p_-). \quad (17)$$

The resulting condensate profile and DCP for a single power density, as well as the pump profile used are presented in Fig. 5(a). In Fig. 5(b), we show the dependence of the DCP, ξ, on the pumping strength above the threshold P/P_{th} for a condensate pumped in a ring. The solution was obtained by numerically solving system (15) for different P and using the spatial averaging of densities across the condensate. The initial pump spin discrepancy was assumed to be 5% ($\eta = 1.05$). The full 2D simulations support the conclusions of Sec. III. The system starts at a synchronized state for small pumping with a high DCP. The desynchronized regime brings the system closer to the linearly polarized state. The synchronized state at high pumping gives the polarization reversal according to the analysis of fixed points of Sec. III.

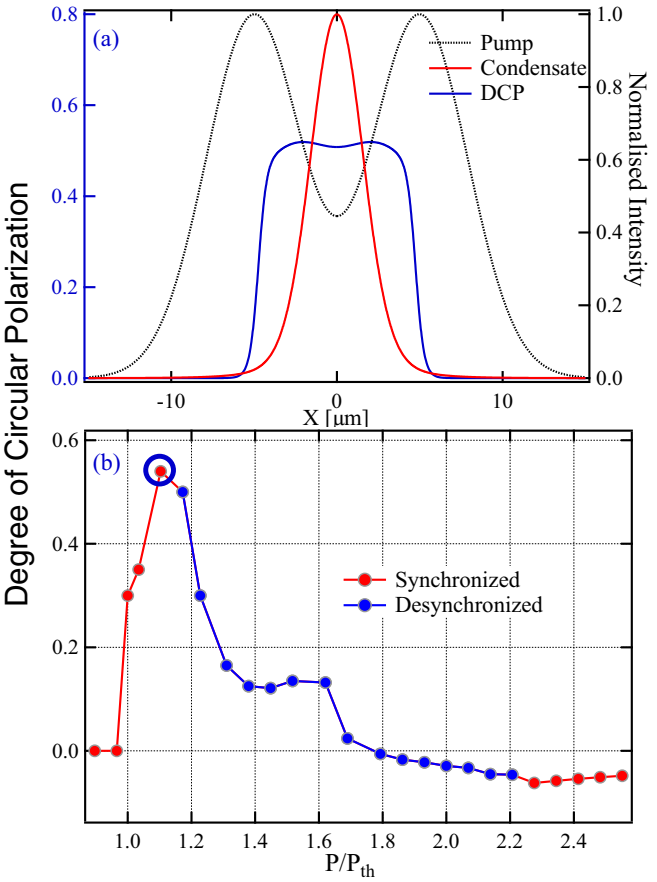

FIG. 5. (a) Simulated pump (dotted black line, right axis) and condensate (solid red line, right axis) real space profile plotted together with the condensate DCP profile (solid blue line, left axis) for $P_{\text{th}} = 1.1$ that has been multiplied by an appropriate hyperbolic tangent function to avoid the irrelevant DCP behavior for the points where the condensate density is too small (less than 10^{-2}). (b) DCP, ξ, as a function of P/P_{th} for a trapped condensate pumped in a ring. The red points correspond to the fixed points, while the blue points to the averaged values of the desynchronized solutions. The blue circle in (b) denotes the point from where the profiles presented in (a) are extracted. Parameters are $\gamma = 10$, $g = 0.7$, $b = 15$, $R = 1.0$, $U_\alpha = 1.1$, $J_{\max} = 0.07$, $\eta = 1.05$, $\alpha = 0.06$, and $r_0 = 5$.

V. CONCLUSIONS

We demonstrate the density dependence of the spin state of a polariton condensate under nonresonant optical excitation. We utilize the spatial separation of the exciton reservoir from the polariton condensate in an annular optical trap scheme, and show the emergence of a strongly polarized spinor condensate. The latter we attribute to the inherent spin imbalance induced by optical excitation in combination with the suppression of spin relaxation through scattering with the exciton reservoir. Most interestingly, we observe a density dependent nonlinear spin reversal at moderate optical excitation densities. The nonlinearity of polariton spin dynamics is described and theoretically reproduced by introducing an internal Josephson coupling term in the spinor GLE, where the dynamics of the system are reduced to a current-driven Josephson junction. We show that the observed spin reversal is due to the interplay between an internal Josephson coupling effect and the detuning of the two projections of the spinor condensate via transition from a synchronized to a desynchronized regime. These results facilitate the design and implementation of polariton based nonlinear spinoptronic devices such as electrically pumped polariton spin switches.

ACKNOWLEDGMENTS

P.G.L. acknowledges support by the Engineering and Physical Sciences Research Council of UK through the Hybrid Polaritonics Programme Grant (EP/M025330/1). P.G.S. acknowledges funding from EU FP7 ERC POLAFLOW, N.G.B. acknowledges the financial support by the Ministry of Education and Science of Russian Federation 1425320 (Project DOI:RFMEFI58114X0006). The authors acknowledge fruitful discussions with Prof. Alexey Kavokin and Dr Hamid Ohadi. All data supporting this study are openly available from the University of Southampton repository at http://eprints.soton.ac.uk/393795/.

[1] I. Žutić, J. Fabian, and S. Das Sarma, Rev. Mod. Phys. **76**, 323 (2004).

[2] T. K. Paraïso, M. Wouters,Y. Léger, F. Morier-Genoud, and B. Deveaud-Plédran, Nat. Mater. **9**, 655 (2010).

[3] S. S. Gavrilov, A. V. Sekretenko, S. I. Novikov, C. Schneider, Höfling, M. Kamp, A. Forchel, and V. D. Kulakovskii, Appl. Phys. Lett. **102**, 011104 (2013).

[4] P. G. Lagoudakis, P. G. Savvidis, J. J. Baumberg, D. M. Whittaker, P. R. Eastham, M. S. Skolnick, and J. S. Roberts, Phys. Rev. B **65**, 161310 (2002).

[5] A. Kavokin, P. G. Lagoudakis, G. Malpuech, and J. J. Baumberg, Phys. Rev. B **67**, 195321 (2003).

[6] P. G. Savvidis, J. J. Baumberg, R. M. Stevenson, M. S. Skolnick, D. M. Whittaker, and J. S. Roberts, Phys. Rev. Lett. **84**, 1547 (2000).

[7] B. Nelsen, G. Liu, M. Steger, D. W. Snoke, R. Balili, K. West, and L. Pfeiffer, Phys. Rev. X **3**, 041015 (2013).

[8] E. Wertz, L. Ferrier, D. D. Solnyshkov, P. Senellart, D. Bajoni, A. Miard, A. Lemaître, G. Malpuech, and J. Bloch, Appl. Phys. Lett. **95**, 051108 (2009).

[9] P. Cilibrizzi, A. Askitopoulos, M. Silva, F. Bastiman, E. Clarke, J. M. Zajac, W. Langbein, and P. G. Lagoudakis, Appl. Phys. Lett. **105**, 191118 (2014).

[10] S. Christopoulos, G. Baldassarri Hoger von Högersthal, A. J. D. Grundy, P. G. Lagoudakis, A. V. Kavokin, J. J. Baumberg, G. Christmann, R. Butté, E. Feltin, J. F. Carlin, and N. Grandjean, Phys. Rev. Lett. **98**, 126405 (2007).

[11] C. Adrados, T. C. H. Liew, A. Amo, M. D. Martín, D. Sanvitto, C. Antón, E. Giacobino, A. Kavokin, A. Bramati, and L. Viña, Phys. Rev. Lett. **107**, 146402 (2011).

[12] T. Gao, P. S. Eldridge, T. C. H. Liew, S. I. Tsintzos, G. Stavrinidis, G. Deligeorgis, Z. Hatzopoulos, and P. G. Savvidis, Phys. Rev. B **85**, 235102 (2012).

[13] D. Ballarini, M. De Giorgi, E. Cancellieri, R. Houdré, E. Giacobino, R. Cingolani, A. Bramati, G. Gigli, and D. Sanvitto, Nat. Commun. **4**, 1778 (2013).

[14] C. Antón, T. C. H. Liew, D. Sarkar, M. D. Martín, Z. Hatzopoulos, P. S. Eldridge, P. G. Savvidis, and L. Viña, Phys. Rev. B **89**, 235312 (2014).

[15] A. Amo, T. C. H. Liew, C. Adrados, R. Houdré, E. Giacobino, A. V. Kavokin, and A. Bramati, Nat. Photon. **4**, 361 (2010).

[16] E. Kammann, T. C. H. Liew, H. Ohadi, P. Cilibrizzi, P. Tsotsis, Z. Hatzopoulos, P. G. Savvidis, A. V. Kavokin, and P. G. Lagoudakis, Phys. Rev. Lett. **109**, 036404 (2012).

[17] C. Antón, S. Morina, T. Gao, P. S. Eldridge, T. C. H. Liew, M. D. Martín, Z. Hatzopoulos, P. G. Savvidis, I. A. Shelykh, and L. Viña, Phys. Rev. B **91**, 075305 (2015).

[18] T. C. H. Liew, A. V. Kavokin, and I. A. Shelykh, Phys. Rev. Lett. **101**, 016402 (2008).

[19] T. Espinosa-Ortega, and T. C. H. Liew, Phys. Rev. B **87**, 195305 (2013).

[20] P. Bhattacharya, B. Xiao, A. Das, S. Bhowmick, and J. Heo, Phys. Rev. Lett. **110**, 206403 (2013).

[21] C. Schneider, A. Rahimi-Iman, N. Y. Kim, J. Fischer, I. G. Savenko, M. Amthor, M. Lermer, A. Wolf, L. Worschech, V. D. Kulakovskii, I. A. Shelykh, M. Kamp, S. Reitzenstein, A. Forchel, Y. Yamamoto, and S. Höfling, Nature **497**, 348 (2013).

[22] J. Cuadra, D. Sarkar, L. Viña, J. M. Hvam, A. Nalitov, D. Solnyshkov, and G. Malpuech, Phys. Rev. B **88**, 235312 (2013).

[23] S. S. Gavrilov, A. S. Brichkin, S. I. Novikov, S. Höfling, C. Schneider, M. Kamp, A. Forchel, and V. D. Kulakovskii, Phys. Rev. B **90**, 235309 (2014).

[24] J. Kasprzak, M. Richard, S. Kundermann, A. Baas, P. Jeambrun, J. M. J. Keeling, F. M. Marchetti, M. H. Szymańska, R. André, J. L. Staehli, V. Savona, P. B. Littlewood, B. Deveaud, and L. S. Dang, Nature **443**, 409 (2006).

[25] F. P. Laussy, I. A. Shelykh, G. Malpuech, and A. Kavokin, Phys. Rev. B **73**, 035315 (2006).

[26] J. J. Baumberg, A. V. Kavokin, S. Christopoulos, A. J. D. Grundy, R. Butté, G. Christmann, D. D. Solnyshkov, G. Malpuech, G. Baldassarri Höger von Högersthal, E. Feltin, J. F. Carlin, and N. Grandjean, Phys. Rev. Lett. **101**, 136409 (2008).

[27] H. Ohadi, E. Kammann, T. C. H. Liew, K. G. Lagoudakis, A. V. Kavokin, and P. G. Lagoudakis, Phys. Rev. Lett. **109**, 016404 (2012).

[28] A. Askitopoulos, H. Ohadi, A. V. Kavokin, Z. Hatzopoulos, P. G. Savvidis, and P. G. Lagoudakis, Phys. Rev. B **88**, 041308 (2013).

[29] A. Askitopoulos, T. C. H. Liew, H. Ohadi, Z. Hatzopoulos, P. G. Savvidis, and P. G. Lagoudakis, Phys. Rev. B **92**, 035305 (2015).

[30] K. V. Kavokin, I. A. Shelykh, A. V. Kavokin, G. Malpuech, and P. Bigenwald, Phys. Rev. Lett. **92**, 017401 (2004).

[31] B. Richards and E. Wolf, Proc. R. Soc. London, Ser. A **253**, 358 (1959).

[32] T. Ha, T. A. Laurence, D. S. Chemla, and S. Weiss, J. Phys. Chem. B **103**, 6839 (1999).

[33] K. Lindfors, A. T. Friberg, T. Setälä, and M. Kaivola, J. Opt. Soc. Am. A **22**, 561 (2005).

[34] P. Cilibrizzi, H. Sigurdsson, T. C. H. Liew, H. Ohadi, S. Wilkinson, A. Askitopoulos, I. A. Shelykh, and P. G. Lagoudakis, Phys. Rev. B **92**, 155308 (2015).

[35] M. M. Glazov, M. A. Semina, E. Y. Sherman, and A. V. Kavokin, Phys. Rev. B **88**, 041309 (2013).

[36] P. Cilibrizzi, H. Sigurdsson, T. C. H. Liew, H. Ohadi, A. Askitopoulos, S. Brodbeck, C. Schneider, I. A. Shelykh, S. Höfling, and P. Lagoudakis, arXiv:1602.04711.

[37] H. Ohadi, A. Dreismann, Y. G. Rubo, F. Pinsker, Y. del Valle-Inclan Redondo, S. I. Tsintzos, Z. Hatzopoulos, P. G. Savvidis, and J. J. Baumberg, Phys. Rev. X **5**, 031002 (2015).

[38] A. Askitopoulos, H. Ohadi, T. C. Liew, Z. Hatzopoulos, P. Savvidis, A. Kavokin, and P. Lagoudakis, in *CLEO: 2014*, OSA Technical Digest (online), (Optical Society of America, Washington, DC, 2014).

[39] A. Fainstein, P. Etchegoin, P. V. Santos, M. Cardona, K. Tötemeyer, and K. Eberl, Phys. Rev. B **50**, 11850 (1994).

[40] A. A. Sirenko, P. Etchegoin, A. Fainstein, K. Eberl, and M. Cardona, Phys. Status Solidi B **215**, 241 (1999).

[41] S. Ohke, T. Umeda, and Y. Cho, Opt. Commun. **70**, 92 (1989).

[42] J. Levrat, R. Butté, T. Christian, M. Glauser, E. Feltin, J. F. Carlin, N. Grandjean, D. Read, A. V. Kavokin, and Y. G. Rubo, Phys. Rev. Lett. **104**, 166402 (2010).

[43] A. Kavokin, G. Malpuech, and M. Glazov, Phys. Rev. Lett. **95**, 136601 (2005).

[44] M. O. Borgh, J. Keeling, and N. G. Berloff, Phys. Rev. B **81**, 235302 (2010).

[45] I. A. Shelykh, D. D. Solnyshkov, G. Pavlovic, and G. Malpuech, Phys. Rev. B **78**, 041302 (2008).

[46] K. G. Lagoudakis, B. Pietka, M. Wouters, R. André, and B. Deveaud-Plédran, Phys. Rev. Lett. **105**, 120403 (2010).

[47] M. Abbarchi, A. Amo, V. G. Sala, D. D. Solnyshkov, H. Flayac, L. Ferrier, I. Sagnes, E. Galopin, A. Lemaître, G. Malpuech, and J. Bloch, Nat. Phys. **9**, 275 (2013).

[48] J. Y. Lien, Y.-N. Chen, N. Ishida, H. B. Chen, C. C. Hwang, and F. Nori, Phys. Rev. B **91**, 024511 (2015).

[49] G. Christmann, G. Tosi, N. G. Berloff, P. Tsotsis, P. S. Eldridge, P. G. Savvidis Zacharias Hatzopoulos, and J. J. Baumberg, New J. Phys. **16**, 103039 (2014).

[50] D. D. Solnyshkov, R. Johne, I. A. Shelykh, and G. Malpuech, Phys. Rev. B **80**, 235303 (2009).

[51] Our dimensional parameters were $\hbar\gamma_C = 0.1$ meV, $\hbar\gamma_R = 1$ meV, $\hbar R_R = 0.1$ meV μm^2, $U_0 = 0.0067$ meV μm^2, and $\hbar g_R = 0.07$ meV μm^2.

[52] M. Wouters, I. Carusotto, and C. Ciuti, Phys. Rev. B **77**, 115340 (2008).

[53] K. G. Lagoudakis, M. Wouters, M. Richard, A. Baas, I. Carusotto, R. André, L. S. Dang, and B. Deveaud-Plédran, Nat. Phys. **4**, 706 (2008).

[54] L. Ge, A. Nersisyan, B. Oztop, and H. E. Tureci, arXiv:1311.4847.

[55] S. H. Strogatz, *Nonlinear Dynamics and Chaos* (Perseus Books, Cambridge, MA, 1994).